Femtosecond ablation scaling for different materials

P. Gonzales, R. Bernath*, J. Duncan, T. Olmstead, M. Richardson
School of Optics/CREOL, University of Central Florida, Orlando, Florida 32816-2700
* rbernat@mail.ucf.edu, Phone (407) 823-6832 ; Fax (407) 823-6880

ABSTRACT

We are making a comprehensive study of the ablation of elemental materials by femtosecond lasers. Specifically, we are examining the ablation of a wide range of metals, under vacuum and in ambient air, using 850-nm wavelength, 100-fs laser pulses in an intensity range approaching and extending beyond the air ionization threshold. We compare ablation rates and examine in detail the morphology and structural integrity of the ablation region, towards gaining greater knowledge of the interaction science as well as constructing empirical models for fabrication guidelines across the periodic table.

Keywords: Femtosecond ablation, elements, metal, foil

1. INTRODUCTION

It is well known that femtosecond lasers have several advantages over conventional laser systems for materials-processing applications. These include the reduction of collateral damage in dielectrics[1], smaller heat-affected zones (HAZ)[2], a deterministic[3] rather than statistically distributed ablation threshold[4], and the ability to ablate sub-diffraction-limited target regions[5]. This has generated increasing interest in the use of femtosecond lasers for precise micro-structuring of a wide range of materials, with applications in medicine, aerospace, microelectronics, photonics, and other industries.

Numerous research and industry groups are working to determine the ablation thresholds for various common materials, such as copper, aluminum, silicon, carbides, oxides, alloys, and various filter materials, as well as the optimization of ablation rates. Recently, our group has experimentally measured the ablation properties of glasses and the ability to micro-machine glass structures.[6-7] Other studies are being conducted on optical filter materials, in the form of glasses and plastics, in the ~1J/cm^2 fluence region using a Ti:Sapphire (Ti^{3+}:Al_2O_3) laser at 800-nm wavelength and 1-kHz repetition rate to examine the effects of high-energy femtosecond pulses. These studies have thus far concluded that the ablation rate of the material is independent of dopant concentration.[8]

Micro-fabrication in metals has long been difficult with lasers due to the high thermal conductivity and low melting points typical of metals. With conventional lasers this has resulted in large heat-affected zones, non-uniform holes, and reformed molten surface debris. This is the result of working in the slow-pulse regime, with pulses greater in length than a nanosecond. Nolte *et al*[5] performed studies on the ablation of metals from the femtosecond pulse-length regime up through picoseconds, including at 150 fs with a Ti:Sapphire laser and fluences of 0.1–10 J/cm^2. This resulted in the first characterization of separate ablation regimes as a function of laser pulse length. With this recognition came the ability to fabricate micro-structures on solid targets with better precision, decreased deposited energy, and less surface damage. Silicon (even though a non-metal) and its compounds are also being studied due to the potential to laser-machine silicon wafers during semiconductor chip manufacturing. Using a Ti:Sapphire laser at 790-nm wavelength with 130-fs pulses under vacuum, researchers have studied the ablation damage to the surface, including the structural details, in a fluence region above the damage threshold. From this it has been verified that at or just above the damage threshold, the silicon tends to melt, and at higher fluences it tends to follow into the ablation regime.[9] Interestingly enough, this implies that the two ablation regimes extend out of the metals and into the non-metals as well.

The two ablation regimes in laser ablation are the multi-photon (skin depth) and the electron diffusion (thermal) regimes. These come out of the Arrhenius-type evaporation equations, and describe the ablation process by

$$L = \delta \ln\left(\frac{F_a}{F_{th}^{Skin}}\right) \text{ where } \delta \approx \alpha^{-1} \tag{1}$$

for low-intensity and

Optical Micro- and Nanometrology in Manufacturing Technology, edited by Christophe Gorecki, Anand K. Asundi, Proceedings of SPIE Vol. 5458 (SPIE, Bellingham, WA, 2004)
0277-786X/04/$15 · doi: 10.1117/12.545927

$$L = l \ln\left(\frac{F_a}{F_{th}^{thermal}}\right) \text{ where } l \approx \sqrt{D\tau_a} \tag{2}$$

for high-intensity ablation.[2] These equations describe the effective drilling depth per shot in terms of the incident laser fluence. For low incident fluences, the skin depth (defined above as δ) defines the effective depth of absorption. For higher laser fluences, the electron thermal diffusion length (defined as *l*) dominates and increases the ablation rate over that of the skin depth.

Many different metals have been examined; in particular, common materials like copper and aluminum which are often machined. Copper is one metal that has been extensively tested due to the frequency of its use, either alone or in combined with other metals in alloys. Ablation of copper foil in air has been studied with an 800-nm, 70-fs laser in the 0.01–28 J/cm^2 regime. In this study, an emphasis was placed on determining the effect of changing the pulse duration, in an attempt to minimize the ablation threshold. As expected, the ablation rate decreased as the pulse length increased.[1, 10] The ablation characteristics of silver, gold, and copper have been studied at fluence levels of 0.1–10 J/cm^2 using a Ti:Sapphire oscillator (780 nm, 120–800 fs) amplified using chirped-pulse amplification (CPA) in Cr^{3+}:$LiSrAlF_6$ (Cr:LiSAF).[11] The researchers used bulk material samples to better simulate and model the effects expected in laser machining, which is usually done on bulk materials rather than foils. In this work, the two ablation regimes (skin depth and electron diffusion) were observed. In addition, they studied the lateral features of the ablated region for use as a precise measurement of ablation ability.[12] Later, the ablation of gold leaf was studied using a frequency-doubled Ti:Sapphire laser (400 nm, 150 fs). Using very low pulse energies, it was found that the laser was able to cut small smooth groves across the surface of the foil. The ablation depth was measured and found to be coupled to the pulse energy. It was also observed that as the pulse energy increased, so did the resulting debris on the surface. We can conclude from this work that to create clean cuts in a metal, the laser pulse energy needs to be below the thermal diffusion length and in the skin-depth regime.[13]

In recent studies, and due to the extensive research already performed on pulse length, greater focus is being placed on the ablation rate's dependence on pulse energy. Wynne *et al* experimented with the ablation rates of aluminum and stainless steel under varying conditions of pulse duration, pulse energy, surface conditions, and ambient atmospheric pressure. They conducted this research with a Ti:Sapphire laser at 810-nm wavelength, 1-kHz repetition rate, 150-fs–40-ps pulse length, and 1.5 mJ energy per pulse. They determined that there was a strong decrease in the ablation rate as the depth of the ablated holes increased, due to surface irregularities forming around the ablated region. These structures tend to inhibit the ablation process by reflecting the light and/or absorbing the energy before it reaches the full depth of the ablated hole, slowing the ablation process. They also found that the ablation rates in air and vacuum are of similar magnitude, but the time required to drill a hole completely through the foil was much shorter in the vacuum regime. They attributed this to the absorption of energy by the plasma plume produced in front of the target, resulting from ionization of the surrounding air.[14] Many groups are currently working on mitigating this effect in order to increase the applied energy and the ablation rate while preserving surface quality. In a related effort, we are investigating the possibility that a multi-pulse scheme might minimize the air ionization, as well as the subsequent parasitic energy absorption and surface degradation; this could result in significantly increased ablation rates.

Zhu *et al* have shown preliminary results that suggest a correlation between the properties of different metals and their ablation rates. They tested aluminum, tungsten, titanium, copper, iron, silver, gold, and lead foils of different thicknesses using a Ti:Sapphire laser at 800 nm and pulse lengths from 60 fs up to nanoseconds. They ablated the samples with equivalent energy but varying pulse length and found three distinct temporal ablation regimes: the femtosecond, the picosecond, and the nanosecond. These regimes correspond to surface shattering, slight melting and ablation of clusters of material, and severe melting of the sample, respectively. From this, they showed that the ablation rates depend on both the laser parameters and the material properties in each of the three different ablation regimes. They report that the material properties affecting the ablation rate are the thermodynamic properties of the material; specifically, the latent energy of evaporation.[15]

With the increasing interest in the use of femtosecond-pulse-length lasers as tools for cutting and ablation, it seems appropriate to create a compendium of laser ablation data for many different elements, with comparisons to their physical parameters, and to establish empirical trends which can be useful for future laser ablation. This paper reports the current status of this study. A more detailed report of these findings will be published at a future date.

2. Experimental setup

For this study, we used part of the LPL Terawatt laser, a 10-TW-peak-power laser consisting of a Ti:Sapphire oscillator followed by a multi-stage CPA Cr:LiSAF amplifier system. For these experiments only the oscillator and a regenerative amplifier were used. The oscillator is a standard 90-MHz Z-cavity design, tuned to 850-nm center wavelength, corresponding to the peak-gain wavelength of Cr:LiSAF. The output of the oscillator is first chirped (stretched in duration) to 200 ps and then amplified by the regenerative amplifier to a maximum of 6 mJ per pulse at 5 Hz. The additional amplifiers in the laser system are bypassed, and the beam is then optically re-compressed to 120 fs and aligned to the target chamber. The variation in the laser energy from pulse to pulse is measured to be approximately 5%. The laser pulse energy is set using a variable attenuator consisting of a Glan-Thompson prism, which also sets the polarization of the laser, in combination with a linear polarizer on a rotation mount. This is done before optical compression to avoid pulse stretching. Using Malus' law,

$$I = I_o \cos^2\left(\theta_{rot}\right) \tag{3}$$

the energy is set to the desired amount.

The samples themselves are various thin foils (from Alfa Aesar and Goodfellow) of at least 99.95% purity, ranging in thickness from 25 μm to 100 μm depending on availability. Each sample is carefully prepared in a clean, dry environment and cut into ¼ by 1 inch rectangles, which are then mounted on special steel substrates. This substrate is then mounted to the sample holder in the chamber. Once ablated, the samples are stored in a clean room to prevent corruption of the surface. The lanthanide materials, which are highly reactive to moisture, require special care and are kept in a positive-pressure dry nitrogen environment to prevent corrosion.

We chose the samples for this experiment such that they are distributed widely across the periodic table (Fig. 1). For this experiment, we used beryllium, titanium, iron, copper, yttrium, molybdenum, silver, gold, tin, lead, neodymium, dysprosium, and ytterbium.

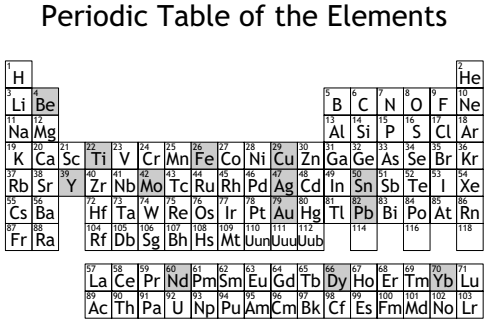

Figure 1. Illustration of chosen elements.

The samples were mounted in the center of the target chamber, affixed to a vacuum-relieved Newport three-axis translation stage assembly, consisting of MFN25PPV6 stages, with a spatial resolution of 1 μm in each direction. The stages are computer-controlled using a Newport MM4006 motion controller, and the ablation is performed in a grid with 250-μm spacing. This comparatively large spacing is to completely isolate each region from debris produced in other regions. We developed a special mount which has an opening directly behind the target region to allow the detection of the laser beam once it has ablated through the foil target. A biconvex 150-mm-focal-length lens was used for this experiment, with an F/# of approximately 6. This lens was chosen rather than a microscope objective to give a larger focal region, decreasing the positioning accuracy required for best focus. The lens produced a measured focal spot of 30-μm FWHM with the Gaussian-profile laser beam. A fast electromechanical shutter was installed in front of the lens, triggered by a fast photodiode directly behind the sample. Dedicated electronics control the starting and stopping of the ablation process by opening the shutter and then closing it as soon as laser light has penetrated the sample. The total number of shots is determined using another fast photodiode which faces the sample and is connected to a high-speed pulse counter. (Fig. 2) Ablation experiments were performed both in vacuum and in air. For the vacuum experiment, a chamber pressure of approximately 10^{-4} torr was used. The polarization of the laser beam is linear TE and is slightly astigmatic, the effects of which can be seen as a non-uniform hole structure in the sample images.

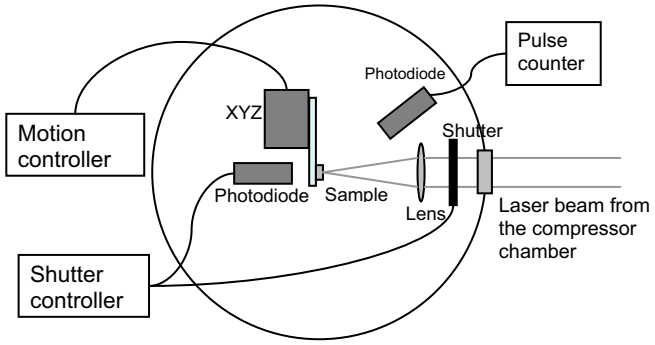

Figure 2. Experimental setup.

To measure the ablation rates of the materials, we ablate the foil samples until the laser beam penetrates completely through to the back surface, counting the number of laser pulses required. For each sample, we used five different energies, and repeated the ablation four times for each energy. We then imaged the sample using an Olympus 20x optical microscope and recorded the front and rear hole diameters, as well as the characteristics of the ablated hole and the surface surrounding the ablation region. From the measured front and rear hole sizes, and knowing that the laser ablates a cone-shaped volume, we then calculated the total volume of ablated material using a conical frustum. From this volume and the known density of the materials, we subsequently calculated the mass removed during ablation. Knowing the number of shots required for break-through and the amount of mass removed, we were then able to determine the average mass removed per shot. This approach ignores the fact that the drilling process is non-linear in nature, and that ablation rates decrease with drilled depth[14]; however, such effects would be difficult to account for until more is known about the exact rate dependence. For the purposes of this comparison, the assumed linearity will not affect the results, as all the samples would have similar dependences.

For these experiments effects of the reflectivities of the different materials were ignored. The intensity region in which we operate is sufficiently high above the ablation threshold that the reflectivity will only affect the initial part of the pulse, causing minor changes to the total energy deposited. Future experiments will consider reflectivity.

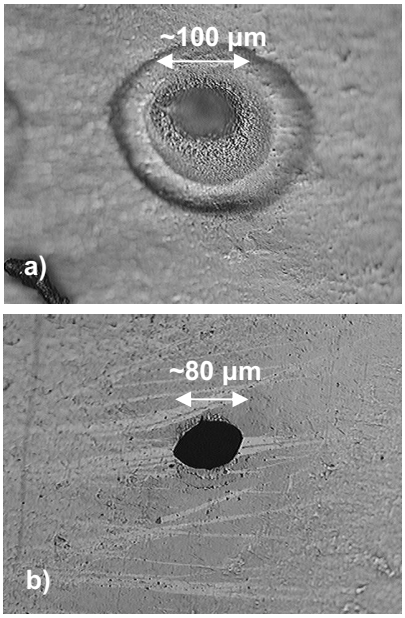

Figure 3. Gold ablated under vacuum at 4 mJ; the result of 73 shots. Front (a) and back (b) sides of sample are shown.

3. Ablation Results

Post mortem analysis of the samples showed signs of operation well above the ablation threshold, with little debris present on the surface and smooth ablated holes. For the thicker samples, and samples with low melting points, there is noticeable material projected from the back surface, which is characteristic of high-temperature melting inside the ablation region.[14] Figure 3 shows images of 25-µm-thick gold ablated with 73 shots at 4 mJ in vacuum. The distinct ring around the hole, which is almost twice the hole's size, is possibly the result of a heat-affected zone or the creation of a thin film on the surface. Since this ablation is performed in vacuum, an oxide layer is unlikely. However, it is interesting that there is no heat-affected zone noticeable on the back surface, which we would expect to see from a localized heat buildup. Future experiments will investigate the nature of this effect. The rough surface inside the hole, which results from tiny beads of reformed molten metal, is characteristic of very hot plasma and the evaporation ablation regime. The lack of debris on the surface indicates that the ablation energies are above those of the melting ablation regime. The asymmetry of the drilled hole can be attributed to two factors: the linear polarization of the laser beam, and a slight astigmatism, which results in an overall oval beam shape. The size of the hole is measured using a computer algorithm which accounts for the shape and provides a best-fit circle for use in our calculations. The gold ablation shown is typical of the ablation seen in vacuum for all samples.

Each sample is ablated at five different energies: 1, 2, 3, 4, and 5 mJ; and the ablation is repeated four times for each energy. The total shot count for each hole is recorded; these counts are averaged and used to calculate the average ablation rate for that energy. The standard deviation of the shot count is used to generate the error bars.

For most samples, the ablation is performed under both vacuum and atmospheric conditions to observe ablation rate dependences on pressure conditions; we have yet to perform vacuum ablation for a few of the samples. The ablation rates are observed to be higher in vacuum than in air. The degree of difference in ablation rate can be observed as variation in the slope of the

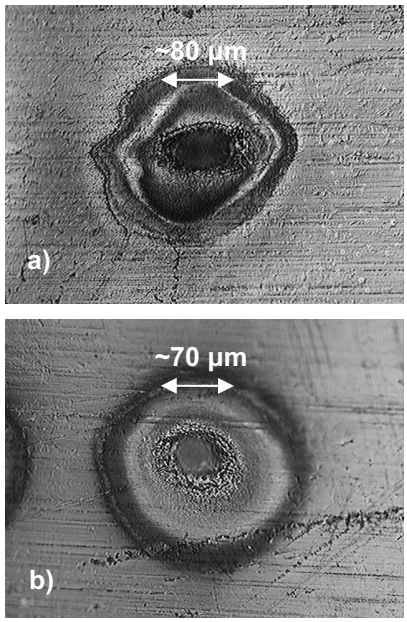

Figure 4. Copper ablation at 5mJ for air (a) and vacuum (b). The numbers of shots are 64 and 43 respectively.

trend. Figure 4 shows copper ablated at 5 mJ in both atmospheric and vacuum conditions. There is a decrease by a third in the number of shots required to ablate through the sample, which agrees with previous results. Note the surface effects on the copper around the ablated hole are similar to those seen on the gold sample. However, the gold sample only showed a color change with no surface deposition or damage. The copper ablated in air shows signs of surface plasma with extensive surface damage and melting. The unusual shape of the outer burn region is likely the result of the astigmatic beam.

4. Discussion

The results from the ablation are compiled and shown in the graphs below. Atmospheric and vacuum ablation rates are plotted on separate graphs as a function of laser pulse energy. The 1–5 mJ region corresponds to intensities from 8×10^{14} to 4×10^{15} W/cm^2 for these focal spot sizes, and is chosen since it is above the ablation thresholds of all the samples and easily produced by the laser.

The first noticeable feature on the measurements taken in air is the large separation of lead and tin from the other elements. The plots of the remaining elements all have varying slopes as shown in Figure 5. The ablation rate of material as a function of pulse energy in this region tends to be approximately linear. For analysis purposes, a best-fit linear regression is applied to each element's data, and is used to find the slope of the trend. This produces an ablation rate figure in terms of mass per shot per energy, also known as Q*.

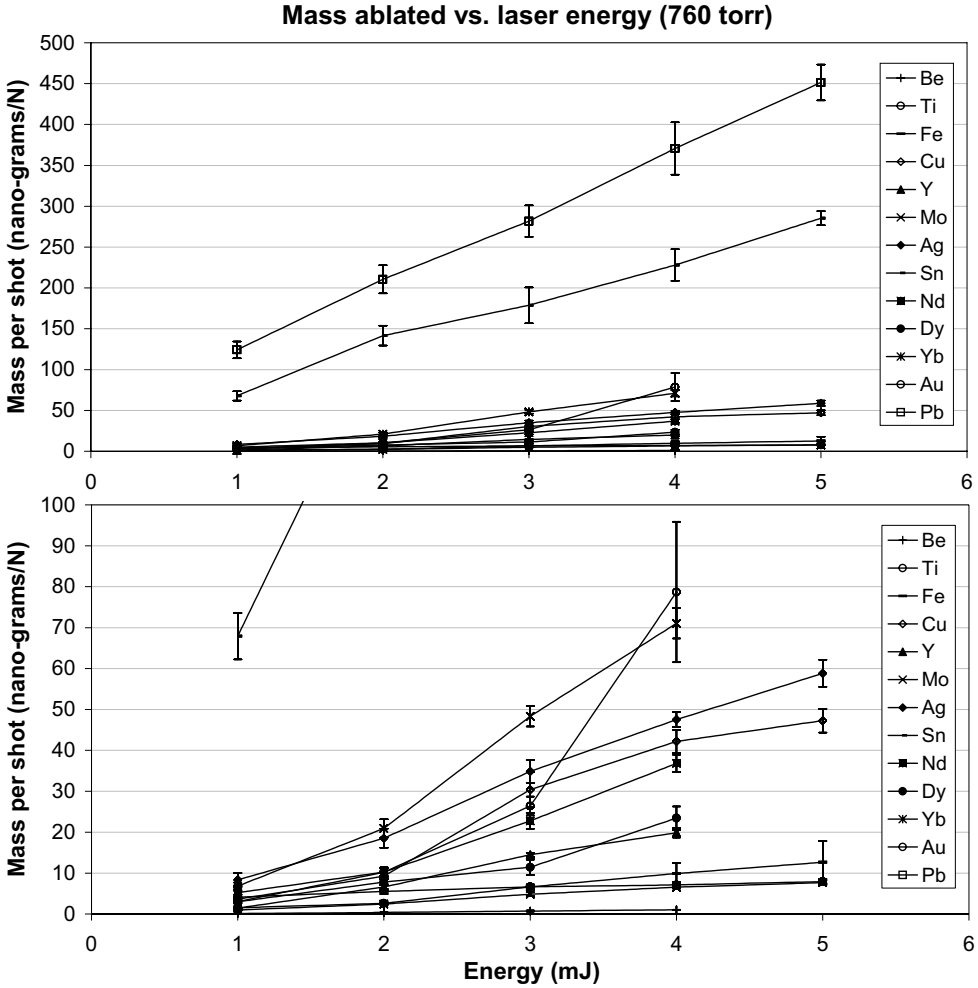

Figure 5. Graphs of mass ablated versus incident energy performed in atmospheric conditions for 13 elements. The top graph shows the full scale while the lower graph shows a close-up of the lower section.

The above graphs show the whole range and a close-up of the lower ablation rates. Note that some of the 5 mJ data points are missing from the chart. This is due to the fact that they did not seem to follow any trend and need to be repeated. This will be performed along with the ablation of additional elements.

Observations from the vacuum ablation experiments show that lead has significantly higher rates than the other elements, whereas tin has a more typical rate (Fig. 6). The higher ablation rates might be due to the low melting points of these two elements. The ablation rates of the elements in vacuum show higher ablated mass per shot than those ablated at atmospheric pressure, which is consistent with known results. The distinct groupings between certain elements, which can be clearly seen in the vacuum ablation chart, attracted our interest. If there is an inherent mechanism causing this grouping, rather than differences in the laser parameters, then it must be some function of the material properties.

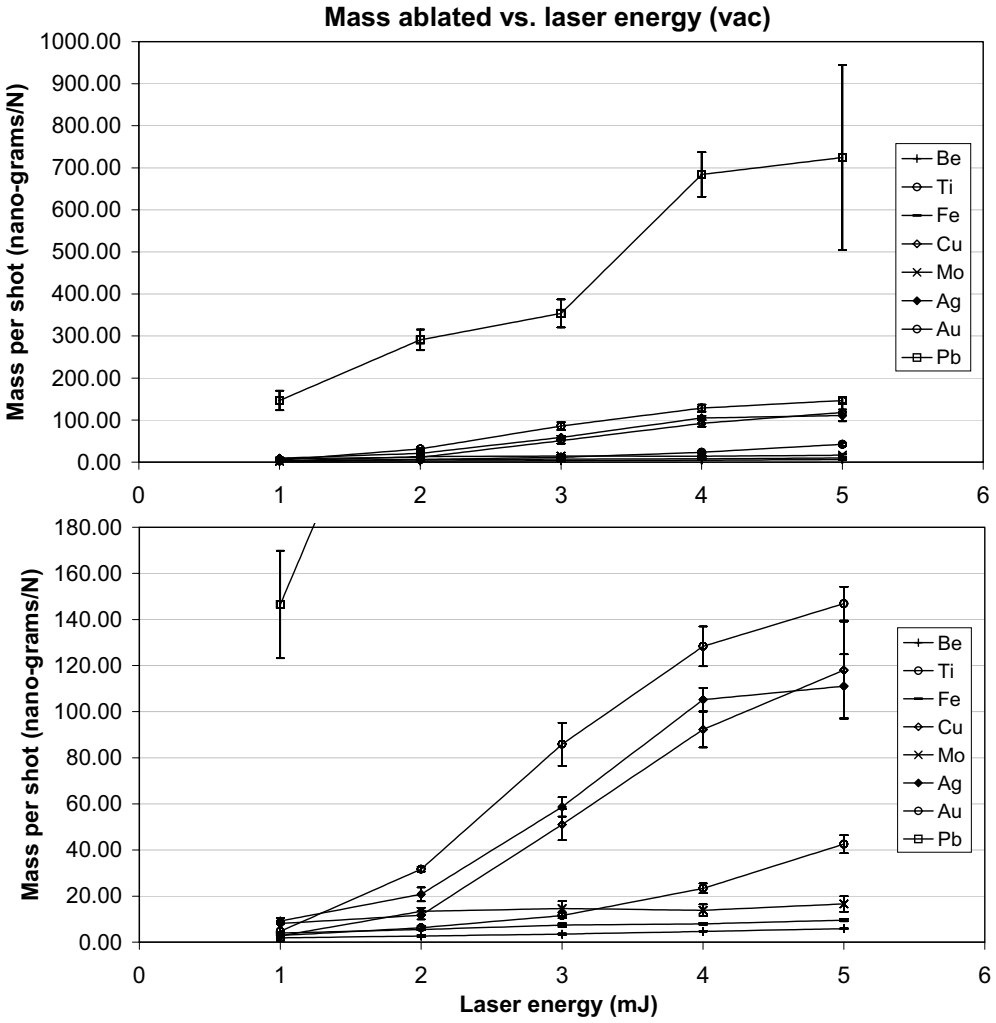

Figure 6. Graph of mass ablated versus incident laser energy for vacuum experiments performed on eight elements. The top graph shows the full scale while the lower graph shows a close-up of the lower section.

A chart was created from the calculated Q* values for both air and vacuum, in combination with common material properties. (Fig. 7) Preliminary observations from this chart indicate that the ablation rate increases with decreasing melting point.

Element		Be	Ti	Fe	Cu	Y	Mo	Ag	Sn	Nd	Dy	Yb	Au	Pb
Z		4	22	26	29	39	42	47	50	60	66	70	79	82
Q* air	ng/mJ	0.313	1.727	2.151	12.007	6.315	1.347	12.996	52.143	10.743	6.491	22.009	12.704	81.463
Q* vac	ng/mJ	0.883	9.632	1.370	31.906	-	4.467	34.606	-	-	-	-	38.085	150.440
ionization	eV	9.3227	6.8281	7.9024	7.7264	6.2171	7.0924	7.5762	7.3439	5.525	5.9389	6.254	9.2255	7.4167
Melting Point	C	1278	1660	1535	1083.4	1523	2617	961.93	231.96	1010	1409	824	1064.43	327.502
Boiling Point	C	2970	3287	2750	2567	3337	4612	2212	2270	3127	2335	1193	2807	1740
Density	g/cm^3	1.848	4.507	7.874	8.92	4.472	10.22	10.491	7.29	6.8	8.551	6.57	19.3	11.34
Resistivity	10^{-8} ·W m	4	40	9.7	1.7	56	5	1.6	11	64	91	28	2.2	21
Thermal Conductivity	W/ (m·K)	190	22	80	400	17	139	430	67	17	11	39	320	35
Thermal expansion	10^6 K	11.3	8.6	11.8	16.5	10.6	4.8	18.9	22	9.6	9.9	26.3	14.2	28.9
Enthalpy of fusion	kJ/mol	7.95	18.7	13.8	13.1	11.4	36	11.3	7	7.1	11.1	7.7	12.5	4.77
Enthalpy of vapor	kJ/mol	297	425	347	300	380	600	255	290	285	280	160	330	178
Enthalpy of atomization	kJ/mol	324	471	415	338	425	659	285	302	328	290	152	368	195

Figure 7. Chart of Q* and known physical data of the elements.

5. Conclusions

Using the LPL terawatt laser system we performed ablation experiments on 13 different elemental materials over energies of 1–5 mJ per pulse. The experiments were performed in atmospheric and vacuum conditions on thin foils ranging from 25 to 100 μm thick. From this experiment we have observed that the ablation rates are higher in vacuum than in air, which agrees with previous work, and that our ablation process occurs at high temperatures. We calculated an average ablation rate in terms of mass per shot per laser energy, which is also known as Q*. Using this information, along with the calculated ablation rates, we can begin to see trends when all the elements are plotted. Others have observed ablation dependences upon the thermodynamic properties of the material; however, our results are inconclusive in that regard. The preliminary results show groupings of the elements by ablation rate as a function of laser energy. To better understand and observe this trend, more samples will be ablated and added to this compendium, and some of the previous samples will be repeated for verification. We also wish to understand why this grouping is very noticeable in the vacuum ablation and not as apparent in the atmospheric ablation data.

In addition, future research will experiment with a burst-mode technique. This involves many low-energy pulses (but with a large total energy) stacked together with very small time separation. The hope is to increase the ablation rate in air, and decrease the severe surface damage, by eliminating the air ionization.

Knowing how the element's physical properties directly affect the ablation rate will provide significant insight into laser machining, laser ablation studies, and the ablation process. With this information it might be possible to predict the ablation results of alloys and other materials where the physical properties are well known.

Acknowledgments

The authors would like to thank the Laser Plasma Laboratory group for their support of and contributions to this effort. We would like to thank Somsak (Tony) Teerawattanasook for his contributions and technical expertise. In addition, we would like to thank our colleagues for all their helpful advice during this project.
Peggy Gonzales participated in this work as an intern from the École Nationale Supérieure de Physique de Marseille, France.

References

1. B.C. Stuart, M.D. Feit, A.M. Rubenchik, B.W. Shore, M.D. Perry, "Laser-Induced Damage in Dielectrics with Nanosecond to Subpicosecond Pulses", *Phys. Rev. Lett*. **74**, 2248, 1995.
2. S. Nolte, C. Momma, H. Jacobs, A. Tunnermann, B.N. Chichkov, B. Wellegehausen, H. Welling, "Ablation of metals by ultrafast laser pulses", *J. Opt. Soc. Am. B,* **14**, 2716, 1997.
3. X. Liu, D. Du, G. Mourou, "Laser ablation and micromachining with ultrashort laser pulses", *IEEE J. of Quantum Electron*. **33**, 1706, 1997.
4. M. Bass, D.W. Fradin, "Surface and bulk laser-damage statistics and the identification of intrinsic breakdown processes", *IEEE J. of Quantum Electron*. **QE-9**, 890, 1973.

5. S. Nolte, B.N. Chichkov, H. Welling, Y Shani, K. Lieberman, H. Terkel, “Nanostructuring with spatially localized femtosecond laser pulses”, *Opt. Lett*. **24**, 914, 1999.
6. L. Shah, J. Tawney, M. Richardson, & K. Richardson, “Femtosecond laser deep hole drilling of silicate glasses in air”, *Applied Surface Science*, **183**, 151-164, 2002.
7. A. Zoubir, L. Shah, K. Richardson & M. Richardson, Proc. SPIE High Power Laser Ablation.
8. J. Kruger, M. Lenzner, S. Martin, M. Lenner, C. Spielmann, A. Fiedler, W. Kautek, “Single- and multi-pulse femtosecond laser ablation of optical filter materials”, *Applied Surface Science*, **208-209**, 233-237, 2003.
9. A.Borowiec, M. Mackenzie, G. C. Weatherly, H. K. Haugen, “Transmission and scanning electron microscopy studies of single femtosecond-laser-pulse ablation of silicon”, *Applied Physics A*, **76**, 201-207, 2003.
10. M. Hashida, A. F. Semerok, O. Gobert, G. Petite, Y. Izawa, J. F. Wagner, “Ablation threshold dependence on pulse duration for copper”, *Applied Surface Science*, **197-198**, 862-867, 2002.
11. P. Beaud, M. Richardson, E. Miesak, B. Chai, "8-TW 90-fs Cr:LiSAF laser", *Optics Letters*, **18-18**, 1550-1552, 1993.
12. K. Furusawa, K. Takahashi, H. Kumagai, K. Midorikawa, M. Obara, “Ablation characteristics of Au, Ag, and Cu metals using a femtosecond Ti:Sapphire laser”, *Applied Physics A*, **69**, S359-S366, 1999.
13. K. Venkatakrishnan, B. Tan, B. K. A. Ngoi, “Femtosecond laser ablation of thin gold films”, *Optics and Laser Technology*, **34**, 199-202, 2002.
14. A. E. Wynne, B. C. Stuart, “Rate dependence of short-pulse laser ablation of metals in air and vacuum”, *Applied Physics A*, **76**, 373-378, 2003.
15. X. Zhu, D. M. Villeneuve, A. Yu. Naumov, S. Nikumb, P. B. Corkum, “Experimental study of drilling sub-10 μm holes in thin metal foils with femtosecond laser pulses”, *Applied Surface Science*, **152**, 138-148, 1999.
16. A. Semerok, C. Dutouquet, “Ultrashort double pulse laser ablation of metals”, *Thin solid films*, **453-454**, 501-505, 2004.